Journal of Materials Science and Chemical Engineering, 2022, 10, 1-15
https://www.scirp.org/journal/msce
ISSN Online: 2327-6053
ISSN Print: 2327-6045

Effect of Substrate Nature on the Structural, Optical and Electrical Properties of In_2S_3 Thin Films

Fethi Aousgi[1*], Youssef Trabelsi[2,3], Aoussaj Sbai[1], Billel Khalfallah[3], Radhouane Chtourou[1]

[1]Laboratory of Nanomaterials and Renewable Energy Systems LaNSER, Research and Technology Center of Energy, Borj-Cedria Science and Technology Park, Hammam-Lif, Tunisia
[2]Physics Department, College of Arts and Sciences in Muhail Asir, King Khalid University, Abha, Saudi Arabia
[3]Laboratory of Photovoltaic and Semiconductor Materials, University of Tunis El Manar, ENIT, Tunis, Tunisia
Email: *aousgifethi@yahoo.fr

How to cite this paper: Aousgi, F., Trabelsi, Y., Sbai, A., Khalfallah, B. and Chtourou, R. (2022) Effect of Substrate Nature on the Structural, Optical and Electrical Properties of In_2S_3 Thin Films. *Journal of Materials Science and Chemical Engineering*, **10**, 1-15.
https://doi.org/10.4236/msce.2022.105001

Received: October 25, 2021
Accepted: May 14, 2022
Published: May 17, 2022

Abstract

In this study, In_2S_3 thin films have been deposited on ITO and fluorine-tin-oxide FTO coated glass substrates by single source vacuum thermal evaporation annealed in vacuum a 300˚C - 400˚C for 1 h. The samples structure was characterized by X-ray diffraction, revealing the quadratic structure of In_2S_3 and the crystallinity depends on the temperature of annealing and nature of substrate. The various structural parameters, such as, crystalline size, dislocation density, strain and texture coefficient were calculated. The optical properties show that the refractive index dispersion data obeyed the single oscillator of the Wemple-DiDomenico model. By using this model, the dispersion parameters and the high-frequency dielectric constant were determined. The Hall Effect has been studied at room temperature. The Hall voltages, the Hall coefficient (RH) and mobility (μH) have been measured at different magnetic and electric fields. The films show n-type behavior irrespective of temperature and composition.

Keywords

In_2S_3, Vacuum Evaporation, Thin Films, X-Ray Diffraction, UV-Vis Spectrophotometer, Photovoltaic

1. Introduction

Indium sulfide (In_2S_3) a typical III - VI group semiconducting chalcogenide with a wide band gap, has received great attention or optoelectronic [1]-[6] photovoltaic [7] [8] [9] and many other applications due to high stability [9], and photoca-

talytic behavior [9] [10] [11].

Indium sulfide (In_2S_3) has been the most widely used in photovoltaic applications due to its excellent photosensitivity and photoconductivity, chemical stability and low toxicity of 2.1 - 2.8 eV [1]-[8]. Recently, the preparation of indium sulfide (In_2S_3) thin films has attracted much attention due to their wide applications in several areas as well as optoelectronic devices [1]-[13]. In_2S_3 exists in three different crystallographic structures: cubic phase (α), tetragonal phase (β) and hexagonal phase (γ). β-In_2S_3 phase is stable at room temperature with stable chemical composition, highly conductivity [11], and intermediate band gaps due to misvalency between sulfur and indium atoms [1] [7] [8]. The binary indium sulfide In_2S_3 was prepared by different methods [1]-[13]. In this work, we present results concerning the fabrication of the In_2S_3 thin films prepared by the thermal vacuum evaporation method.

Herein, we report the influence of substrates nature and annealing in vacuum at 300˚C and 400˚C on β-In_2S_3 thin films. In addition, the optical and electrical properties, crystallographic structure and phase purity of In_2S_3 thin films were investigated in detail. These measurements check the consistency of the materials for some specific applications. An attempt has been done to highlight the optical features of the thin film alloys. The dispersion parameters were estimated according to the Wemple-Di Domenico model.

2. Experimental Sections

Thin films of In_2S_3 have been deposited by single source vacuum thermal evaporation onto tin oxide (ITO) and onto fluorine-doped tin oxide (FTO) coated glass substrate and annealed in vacuum at different temperature 300˚C and 400˚C for 1 h. The substrates were placed directly above the source at a distance of 15 cm. The vacuum chamber was evacuated to 10^{-6} Torr before the source was heated. Then, the films were removed after waiting for a few hours for the chamber to cool down. The film thickness was varied from 300 to 600 nm was controlled and monitored during the evaporation process by using a quartz crystal sensor (Model, TM-350 MAXTEK, 0Inc., USA).

Samples were characterized by X-ray diffraction (XRD, Philips PW 3710) (Cu-Kα radiation, from 10˚ - 70˚ in 2θ) for a scanning speed of the XRD test of 1 hour. The average size of the crystallites was calculated by using the Debye-Scherrer formula. The optical properties of the prepared samples were investigated by UV-Vis Shimadzu UV 3100S spectrophotometer a double-beam in the wavelength range of 300 - 1800 nm. Finally, the electrical properties were studied using by Hall Effect.

3. Results and Discussions

3.1. Structural Analysis

Figure 1 show the XRD patterns of In_2S_3 thin films on ITO and fluorine-tin-oxide FTO coated glass substrates with various thicknesses before vacuum an-

nealing. From **Figure 1**, it can be also seen that, all the layers are amorphous, the reflexions marked by (*) in the patterns are assigned to the ITO and FTO coated glass substrates. This result was in agreement with those results in the literature [14] [15] [16] [17].

The XRD patterns of the different samples are shown in **Figure 2(a)**. The In_2S_3/ITO and FTO films are annealed at 300˚C and 400˚C. The first observable effect is the appearance of the characteristic basal reflections of In_2S_3. The diffraction maxima of 2θ at 27.55, which correspond to the (109) reflection ascribed to In_2S_3 quadratic (JCPDS Card no. 782486) appear with hight intensity in all the samples. After annealing, all the XRD patterns just show the diffraction maxima of the quadratic spinel phase (JCPDS id. 78-2486) with (109) preferential orientation. This result is in good agreement with other studies [18] [19] [20] [21]. However, herein, the annealing of films at different temperature affects the crystallization of In_2S_3. Pointing out the intensity and shape of the In_2S_3 reflection maxima, it is clear that the crystallinity of the In_2S_3 formed varies depending on the nature of substrate ITO and FTO (**Figure 2(a)**).

Figure 2(b) depicts the diffractograms of indium sulfide on ITO and FTO layers with about 650 nm thickness. We can observe that the (103) peak becomes sharper in the films deposited on ITO substrates compared to the deposited on FTO substrates. In other side, the crystallinity of the In_2S_3 is enhanced with the temperature of annealing increase (400˚C) and the best crystallinity is obtained for a deposition on ITO substrate. Also, it can be also noticed, a slight shift of the main diffraction maxima when the annealing temperature increases from 300˚C to 400˚C (Inset **Figure 2(b)**). It can be attributed to a decrease in stress with generates a decrease in the dislocation [22]. This result can be explained by the rearrangement of the atoms into a lower energy state corresponding to a more orderly arrangement.

The average crystallite size can be estimated using Scherer's formula:

$$D = \frac{0.9\lambda}{\beta \cos\theta} \tag{3}$$

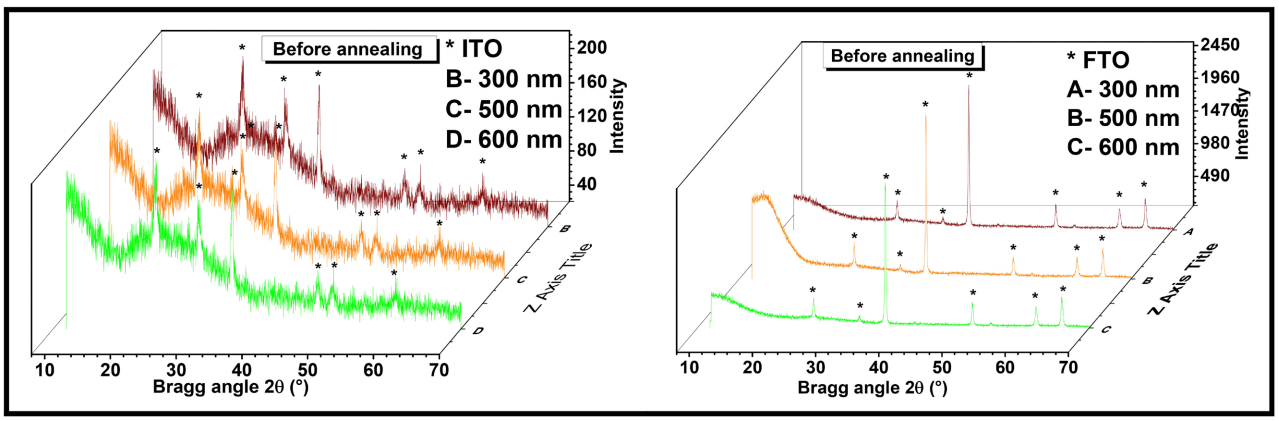

Figure 1. X-ray diffraction spectra of the In_2S_3 thin films deposited on to ITO and FTO glass substrates non-annealing at different thicknesses.

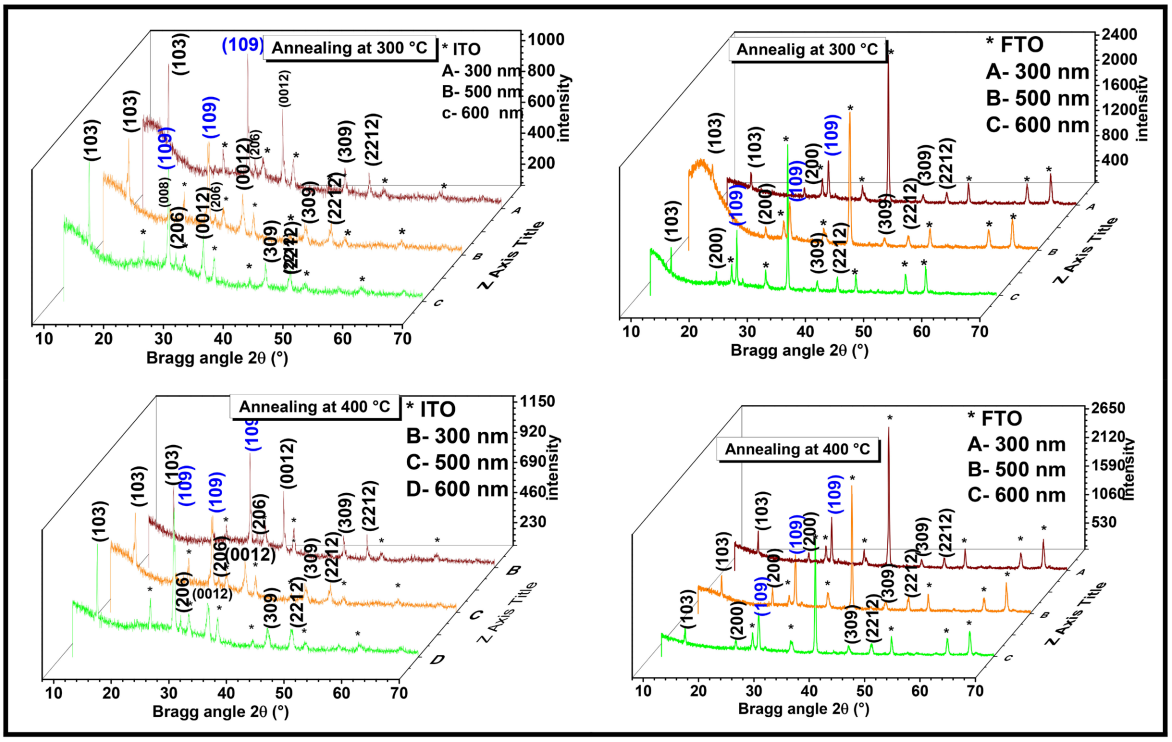

(a)

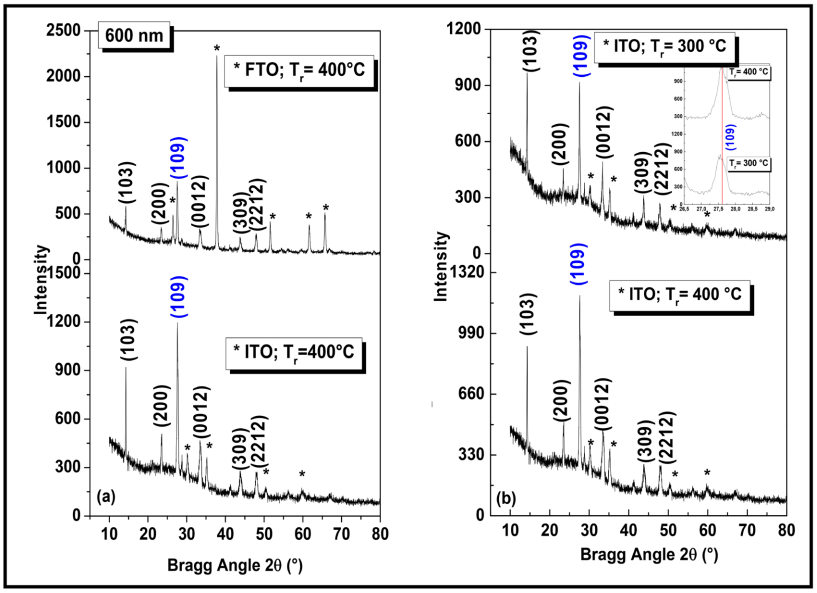

(b)

Figure 2. (a) X-ray diffraction spectra of the In_2S_3 thin films deposited on to ITO and FTO glass substrates annealing at 300˚C and 400˚C for different thicknesses; (b) X-ray diffraction spectra of the In_2S_3 thin films deposited on to ITO and FTO glass substrates annealing at 300˚C and 400˚C with the thickness of 600 nm.

where λ (0.1541 nm) is the wavelength of Cu Kα radiation, θ is the Bragg angle, and β is the half-width at half maximum (HWHM) of the diffraction maxima (109). Table 1 collects the In_2S_3 crystal size values estimated by the Scherrer's equation.

Table 1. Evolution of the crystallite size of In_2S_3 thin films deposited with different thickness onto ITO and FTO substrates and annealing at 300˚C and 400˚C.

Annealing Temperature (˚C)	thickness (nm)	crystallite size (Å)	
		ITO Substrates	FTO Substrates
300	300	66.1	45.3
	500	79.8	55.2
	600	82.1	61.6
400	300	102.4	96.1
	500	145.8	114.9
	600	151.2	122.4

3.2. Optical Properties

Figure 3 displays the transmission and reflexion spectra of the prepared samples before annealing.

The results show that the transmission value varying from 80% to 70% correspond to In_2S_3 deposited on ITO and FTO coated glass substrates, respectively. As well as, the total reflexion value at 45% and 40% correspond to ITO and FTO coated glass substrates respectively.

Figure 4(a) and **Figure 4(b)** displays the transmission and reflxion of the samples annealing at 300˚C and 400˚C for 1 hours of the In_2S_3 deposited on ITO and FTO coated glass substrates.

From **Figure 4**, it can be also seen that, the low variation of transmittance after thermal treatment showing interference fringes, can be attributed to the homogeneity of In_2S_3 thin films.

Transmission spectra for layers deposited on the ITO show interference fringes, indicating good homogeneity. The transmission reaches 95% in the visible and near infrared range (**Figure 4(b)**). It is most important for the 300 nm thick layer. For those deposited with FTO, the transmission decreases dramatically indicating an aspect of inhomogeneity. We also note a decrease in the transmission values for the layers deposited at the FTO by about 25% compared to the layer deposited at the ITO. We explain the decrease in transmittance values for layers deposited at FTO compared to those deposited on ITO by the difference in structural condition and surface condition for each substrate.

The relation between the absorption coefficient, α, and the incident photon energy, $h\nu$, can be written as:

$$(\alpha h\nu) = A\left(h\nu - E_g\right)^n \tag{3}$$

where A is a constant and n is a number which characterizes the transition process. The value, $n = 1/2$, characterizes a direct allowed optical transition. Plotting of $(\alpha h\nu)^2$ versus photon energy, $h\nu$, yields a straight line indicating direct optical transition. The band gap values were obtained from the transmission spectra of In_2S_3 thin films for different thickness on ITO and FTO-coated glass substrates. The values of the direct band gap E_g are collected in **Table 2**. These

values show that the optical gap decreases with the thickness of the layers for both types of substrates. This related to the degree of non-stoichiometry of In_2S_3 for low thicknesses and to the increase in crystallinity for large thicknesses. The corresponding E_g values calculated for the thin films of ITO and FTO decreases according to the thickness of the layers from 2.01 to 2.8 eV, which is close to that reported in the bibliography [23] [24] [25] [26] (2.5 eV).

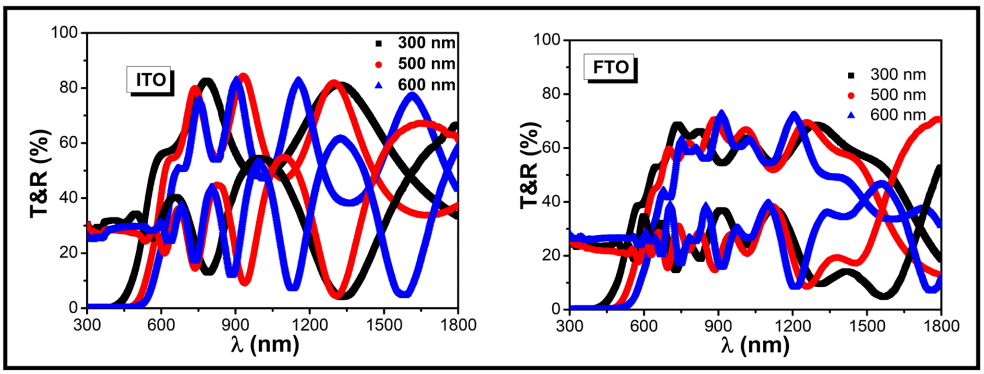

Figure 3. Optical transmission and reflection spectra of In_2S_3 thin films with different thicknesses deposed on ITO and FTO coated glass substrates.

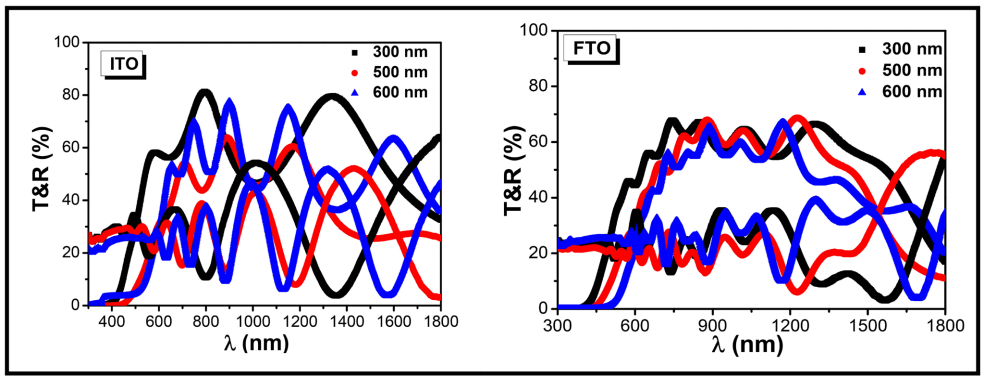

(a)

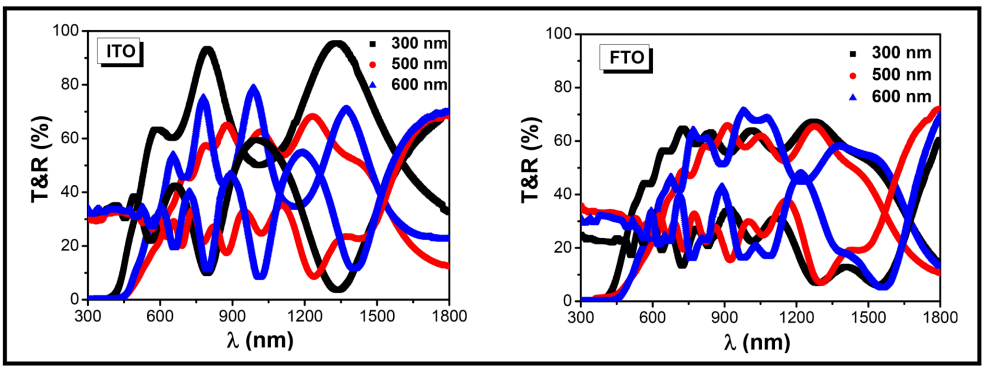

(b)

Figure 4. (a) Optical transmission and reflection spectra of In2S3 thin films with different thicknesses after vacuum annealing at 300˚C deposed on ITO and FTO coated glass substrates; (b) Optical transmission and reflection spectra of In_2S_3 thin films with different thicknesses after vacuum annealing at 400˚C deposed on ITO and FTO coated glass substrates.

Table 2. Estimated values of the optical band gap of In_2S_3 thin films with different thicknesses before and after vacuum annealing at 300˚C and 400˚C deposed on ITO and FTO coated glass substrates.

Thickness (nm)		300		500		600	
		ITO	FTO	ITO	FTO	ITO	FTO
E_g (eV)	Before annealing	2.74	2.62	2.47	2.51	2.35	2.01
	Annealing at 300˚C	2.66	2.8	2.62	2.75	2.04	2.50
	Annealing at 400˚C	2.65	2.64	2.63	2.61	2.56	2.25

Also, the refractive index, n of In_2S_3 films was calculated through the transmission maxima, T_M and minima, T_m of the envelopes of the transmission spectra, by using the Swanepoel method [27] [28].

$$n = \left[N + \left(N^2 - n_s^2 \right)^{1/2} \right]^{1/2} \tag{3}$$

With

$$N = \frac{2n_s \left(T_M - T_m \right)}{T_M T_m} + \frac{n_s^2 + 1}{2} \tag{4}$$

s is the refractive index of the glass substrate and T_M and T_m represent the envelopes of the maximum and minimum positions of the transmission spectra.

The variations of refractive index $n(\lambda)$, with Cauchy fitting for In_2S_3 thin films with different thicknesses are shown in **Figure 5** and **Figure 6**, respectively. It is clear seen, that the refractive indices variations obey to the Cauchy decreases with increase of wavelength and remains constant above 1000 nm showing normal dispersion law for all the films [29]. The initial sharp decrease of n with wavelength indicated a rapid change in the absorption energy of the material [30], which depends on the surface and volume imperfections [31]. The average refractive indices values were in range 1.79 - 3.02 for the all the films (**Table 3**). These refractive indices values were taken for wavelengths greater than 1000 nm which corresponds to the spectral transparency region. The increase of refractive index indicates the improvement in the crystallinity of the films that could be decreased during the deposition process itself with the increase of thickness at different annealing deposed on ITO and FTO coated glass substrates so that the films had a better crystallinity leading to higher refractive index. Also, the variation in refractive index can be attributed to the changes occurring in the strain and dislocation density of the layers [32].

The Cauchy's formula of the refractive index n, as a function of the wavelength λ, is [33] [34].

$$n(\lambda) = n_0 + \frac{A}{\lambda^2} + \frac{B}{\lambda^4} \tag{5}$$

where n_0, A and B are the Cauchy's parameters and λ is the wavelength.

According to the Cauchy distribution, the refractive index depends on the

material and the wavelength. The best fit of experimental data was added in Figure 6. The values of Cauchy's parameters are gathered in Table 3.

According to Cauchy's formula, we can noticed that a non-dispersive medium, $A = B = 0$ and that a medium is less and less dispersive if these constants tend towards zero at the same time. As well as, it is observed that for these constants are very far from zero despite the fact that some decrease slightly in some layers deposited on FTO substrates. This proves the dispersive character of these materials.

Wemple and DiDomenico [35] [36] have developed a model where the refractive index dispersion is studied in the region of transparency below the gap, using the single effective oscillator approximation. It is well known from the dispersion theory that in the region of low absorption the refractive index n described to a very good approximation, by the following formula,

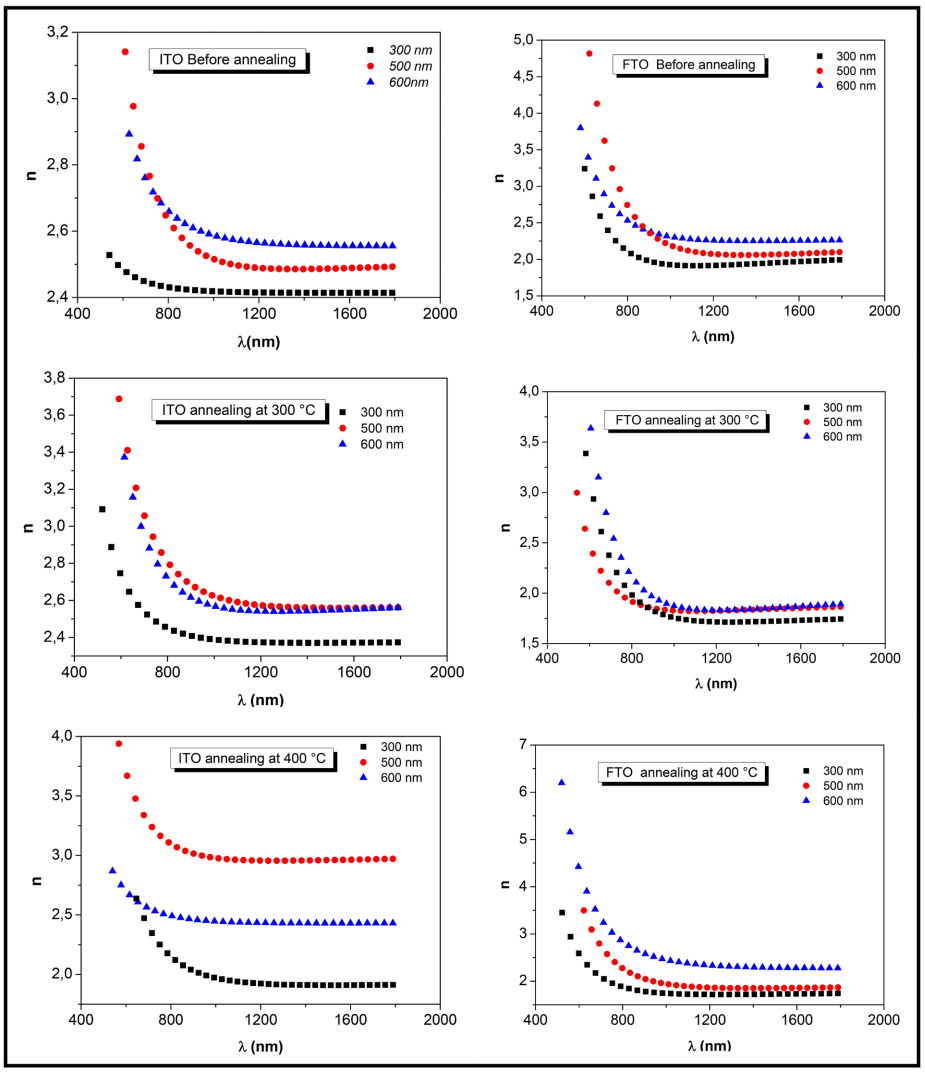

Figure 5. Spectral dependence of the refractive index n of In_2S_3 thin films with different thicknesses before and after vacuum annealing at 300˚C and 400˚C deposed on ITO and FTO coated glass substrates.

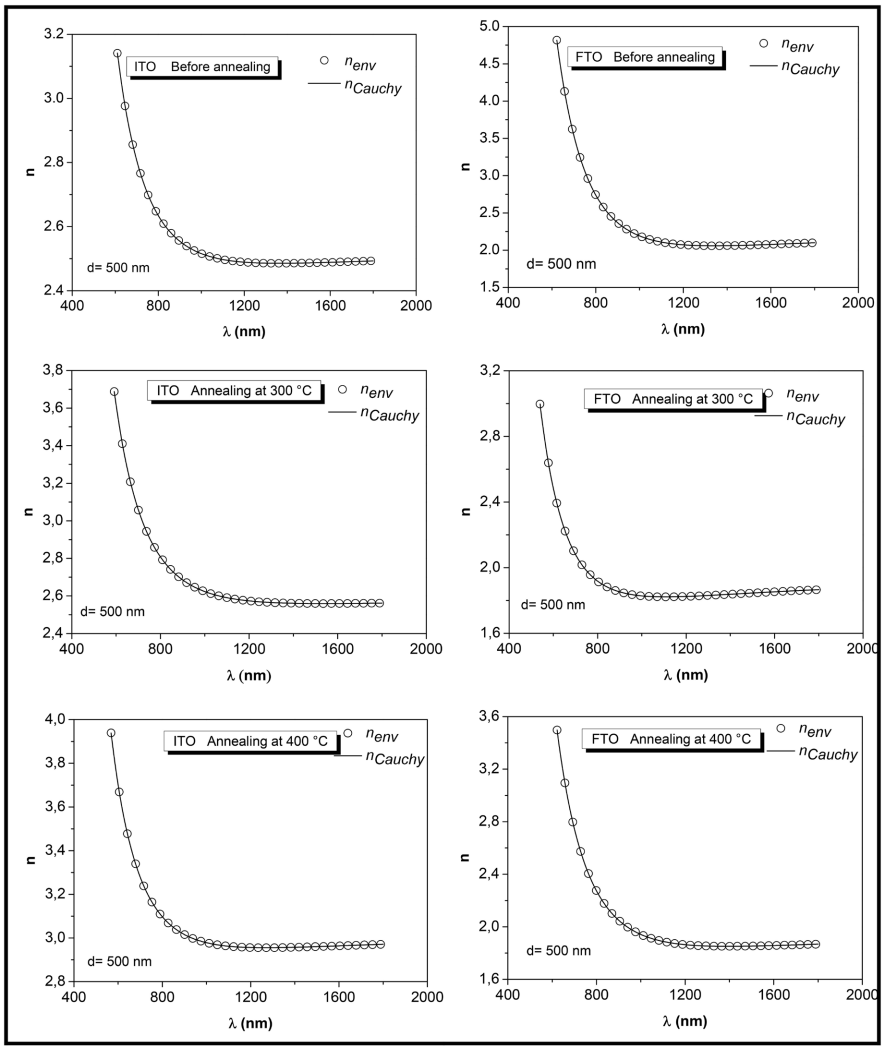

Figure 6. Variation of the refractive index $n(\lambda)$ with wavelength of In_2S_3 thin films deposed on ITO and FTO coated glass substrates at 500 nm before and after vacuum annealing.

Table 3. Estimated values of the Cauchy constants of In_2S_3 thin films with different thicknesses before and after vacuum annealing at 300˚C and 400˚C deposed on ITO and FTO coated glass substrates.

Heat treatment	Thickness (nm)	n_0		A (μm^2)		B (10^7 μm^4)	
		ITO	FTO	ITO	FTO	ITO	FTO
Before annealing	300	2.41	2.12	−0.096	−0.542	0.12	3.39
	500	2.52	2.26	−0.153	−0.743	1.42	6.69
	600	2.56	2.32	−0.043	−0.268	0.68	2.57
Annealing at 300˚C	300	2.38	1.83	−0.070	−0.386	0.71	3.09
	500	2.59	1.93	−0.160	−0.280	1.91	1.72
	600	2.62	2.03	−0.256	−0.596	2.04	4.35
Annealing at 400˚C	300	1.94	1.79	−0.163	−0.245	1.89	1.89
	500	3.02	1.95	−0.199	−0.396	1.60	3.84
	600	2.43	2.30	−0.042	−0.018	0.49	3.34

$$n^2(h\nu) = 1 + \frac{E_d E_0}{E_0^2 - (h\nu)^2} \quad (6)$$

where, $h\nu$ is the photon energy, E_0 is the single oscillator energy and E_d is the dispersion energy.

Plotting $(n^2 - 1)^{-1}$ against $(h\nu)^2$ (Figure 7) allow us to determine the oscillator parameters by fitting a straight line to the points. The values of E_0 and E_d can be determined directly from the slope $(E_0E_d)^{-1}$ and the intercept on the vertical axis, (E_0/E_d). It was found that E_d varies between 4.29 and 36.8 eV and E_0 varies from 2.23 to 7.74 eV for the different substrate.

The high-frequency dielectric constant ε_∞ is obtained by the Wemple-Didomenico model by stretching $h\nu \to \infty$:

$$\varepsilon_\infty = 1 + \frac{E_d}{E_0} \quad (7)$$

The different values of the oscillator parameters were summarized in Table 4.

The effect of the nature of the substrate reveals that the E_d dispersion energies are marked by a drop for layers deposited on FTO substrates (e.g. from 36.8 eV for unannealed layers deposited on ITO substrates to 6.7 eV for layers deposited on FTO substrates). Similarly for the average energy E_0 describes a decrease for layers deposited on FTO compared to ITO.

The effect of the nature of the substrate reveals that the Ed dispersion energies are marked by a drop for layers deposited on FTO substrates (e.g. from 36.8 eV for unannealed layers deposited on ITO substrates to 6.7 eV for layers deposited on FTO substrates). Similarly for the average energy E_0 describes a decrease for layers deposited on FTO compared to ITO.

Table 4. The estimated values of the oscillator parameters E_0 and E_d, the value of the refractive index and ε_∞ as well as other related optical parameters extrapolated from the Wemple-Di Domenico model.

Heat treatment	Thickness (nm)	E_d (eV)		E_0 (eV)		ε_∞	
		ITO	FTO	ITO	FTO	ITO	FTO
Before annealing	300	36.80	6.72	7.74	2.23	5.75	4.01
	500	25.78	6.25	4.76	2.75	6.41	3.27
	600	18.44	9.21	3.87	2.58	5.76	4.57
Annealing at 300˚C	300	15.92	4.29	3.69	2.53	5.31	2.69
	500	16.79	6.21	3.31	2.93	6.07	3.12
	600	19.04	5.47	3.75	2.61	6.07	3.09
Annealing at 400˚C	300	26.82	4.44	3.72	2.58	8.21	2.72
	500	19.68	5.63	4.22	2.65	5.66	3.12
	600	7.55	9.07	3.15	2.44	3.39	4.71

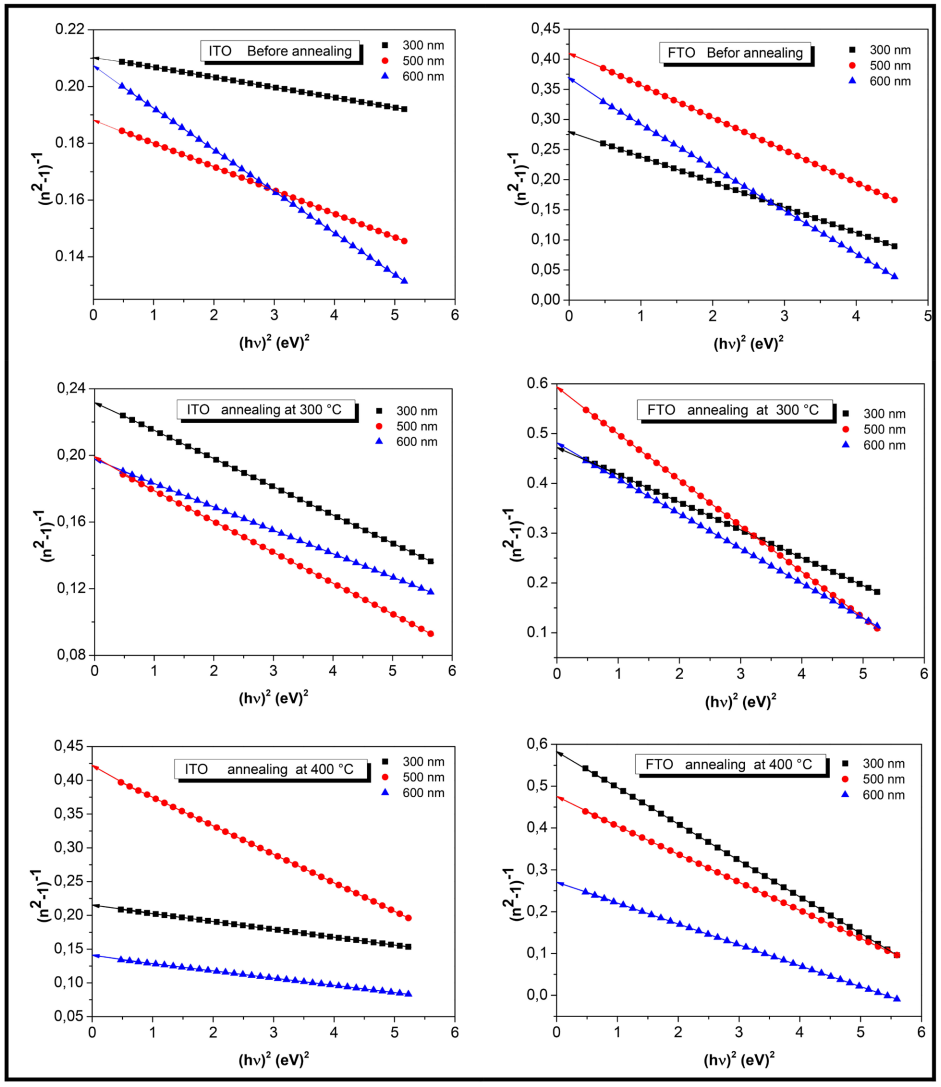

Figure 7. Plot of $(n^2 - 1)^{-1}$ against $(h\nu)^2$.

3.3. Electrical Properties

The optoelectronic properties investigated by Hall Effect shows very intersting result. In fact, the nature of the substrate as well as the heat treatment under vaccum plays an essential role. The electrical properties of the samples with different annealing temperature and thickness are shown in **Table 5**. The Hall Effect study confirmed that layers have a very significant density out of carrier's loads indicating a semiconductor n-type, which shows that the thermal treatment and substrate type do not change the type of the majority carriers in β-In_2S_3 [37]-[43]. Before annealing, they films deposited at FTO substrats present the highest resistivity and mobility. But after annealing treatment at 300˚C - 400˚C, on notice another behavior of the resistivity of the β-In_2S_3 thin films deposited at ITO. In fact, it can be observed that the ITO substrate is more stable and gives layers that have the lowest, resistivity. This resultas, it is on correlation with the XRD investigation wich shows that they films deposited at ITO

Table 5. Estimated values of the electrical properties of β-In_2S_3 thin films with different thicknesses before and after vacuum annealing at 300˚C and 400˚C deposed on ITO and FTO coated glass substrates.

Heat treatment	Thickness (nm)	d ($cm^{-3} \times 10^{20}$)		ρ ($\Omega cm \times 10^{-4}$)		μ ($cm^2/V.S$)	
		ITO	FTO	ITO	FTO	ITO	FTO
Before annealing	300	−1.44	−2.25	14.32	2.63	3.8	10.5
	500	−3.27	−6.19	6.44	3.12	29.6	32.3
	600	−2.18	−3.03	8.87	5.45	32.1	37.7
Annealing at 300˚C	300	−5.30	−4.24	4.19	2.14	28.1	68.5
	500	−5.80	−1.93	5.52	14.23	19.5	38.4
	600	−6.36	−0.01	4.40	28.8	17.3	22.2
Annealing at 400˚C	300	−4.69	−0.04	3.75	28.2	35.4	173.9
	500	−6.05	−4.47	3.68	5.16	17.9	27.1
	600	−5.03	−9.01	5.69	3.36	10.8	17.2

N.B: *d*: carriers density; ρ: resistivity and μ: mobility.

substrats present the high crystallinity compared to FTO substrates. Indeed the influence of the substrate is better felt for the indium sulfide layers on ITO. We also notice that the carrier concentration is important for both series of samples.

4. Conclusion

In this study, the effect of substrate nature on the structural, optical and electrical properties of In_2S_3 thin films deposited by single source vacuum thermal evaporation onto ITO and fluorine-tin-oxide FTO coated glass substrate. The parameters are optimized to yield uniform and well adhering films. The experimental characterization indicates that the substrate nature and vacuum annealing play an important role in the structural, optical and electrical properties of the films. All the In_2S_3 films are polycrystalline in nature after annealed under vacuum at 60 minutes and exhibit an tetragonal crystal structure with preferred grain orientation along (1 0 9) plane. The band gap energy of the films was found to be decreased from 2.74 to 2.01 eV for ITO and from 2.8 to 1.94 for FTO by increasing the thicknesses of the films.

The refractive index n of the In_2S_3 films was found to be dependant of the substrate nature. The refractive index and the single-oscillator parameters were calculated and discussed considering the Wemple-DiDomenico model. The results have shown that the band gap energy E_g, the oscillator energy E_0, and dispersion energy E_d, are strongly dependent on substrate nature. Moreover, these films have an n-type electrical conductivity of approximately 10^{-3} $S \cdot cm^{-1}$.

Acknowledgements

The authors are thankful to the Deanship of Scientific Research—Research Center at King Khalid University in Saudi Arabia for funding this research (Code Number: R.G.P.1/322/42).

Conflicts of Interest

The authors declare no conflicts of interest regarding the publication of this paper.

References

[1] Gopinath, G.R., Miles, R.W. and Reddy, K.T.R. (2013) Influence of Bath Temperature on the Properties of In_2S_3 Films Grown by Chemical Bath Deposition. *Energy Procedia*, **34**, 399-406. https://doi.org/10.1016/j.egypro.2013.06.768

[2] Takatori, K., Nishino, T., Okamoto, T., *et al.* (2016) Indium-Free Organic Thin-Film Solar Cells Using a Plasmonic Electrode. *Journal of Physics D: Applied Physics*, **49**, Article ID: 185106. https://doi.org/10.1088/0022-3727/49/18/185106

[3] Asenjo, B., Guilln, C., Chaparro, A.M., Saucedo, E., Bermudez, V., Lincot, D., Herrero, J. and Gutirrez, M.T. (2010) Properties of In_2S_3 thin Films Deposited onto ITO/Glass Substrates by Chemical Bath Deposition. *Journal of Physics and Chemistry of Solids*, **71**, 1629-1633. https://doi.org/10.1016/j.jpcs.2010.09.011

[4] Aslan, F., Adam, G., Stadler, P., Goktas, A., Mutlu, I.H. and Sariciftci, N.S. (2014) Sol-Gel Derived In_2S_3 Buffer Layers for Inverted Organic Photovoltaic Cells. *Solar Energy*, **108**, 230-237. https://doi.org/10.1016/j.solener.2014.07.011

[5] Gololobov, Y.G. and Kasukhin, L.F. (1992) Recent Advances in the Staudinger Reaction. *Tetrahedron*, **48**, 1353-1406. https://doi.org/10.1016/S0040-4020(01)92229-X

[6] William, J.A. (1993) Ylides and Imines of Phosphorus. Wiley, New York, 597-614.

[7] Thomas, T., Kumar, K.R., Kartha, C.S. and Vijayakumar, K.P. (2015) Simple One Step Spray Process for $CuInS_2/In_2S_3$ Heterojunctions on Flexible Substrates for Photovoltaic Applications. *Proceedings of SPIE*, **9561**, 95610J. https://doi.org/10.1117/12.2187065

[8] Gao, Z., Liu, J. and Wang, H. (2012) Investigation on Growth of In_2S_3 thin Films by Chemical Bath Deposition. *Materials Science in Semiconductor Processing*, **15**, 187-193. https://doi.org/10.1016/j.mssp.2012.02.004

[9] Qiu, H., Fang, S., Huang, G. and Bi, J. (2020) A Novel Application of In_2S_3 for Visible-Light-Driven Photocatalytic Inactivation of Bacteria: Kinetics, Stability, Toxicity and Mechanism. *Environmental Research*, **190**, Article ID: 110018. https://doi.org/10.1016/j.envres.2020.110018

[10] Zhao, W., Huang, Y., Su, C., Gao, Y. and Tian, W., Yang, X. (2020) Fabrication of Magnetic and Recyclable $In_2S_3/ZnFe_2O_4$ Nanocomposites for Visible Light Photocatalytic Activity Enhancement. *Materials Research Express*, **7**, Article ID: 015080. https://doi.org/10.1088/2053-1591/ab6aca

[11] Nefzi, C., Souli, M., Castilla, M.L.D., García, J.M. and Kamoun-Turki, N. (2020) Structure d'hétérojonction CFTS-3/In_2S_3 /SnO_2: F en tant que candidat photocatalytique écologique pour éliminer les polluants organiques. *Arabian Journal of Chemistry*, **13**, 6366-6378. https://doi.org/10.1016/j.arabjc.2020.05.038

[12] Chate, P.A., Sathe, D.J., Hankare, P.P., Lakade, S.D. and Bhabad, V.D. (2015) β-In_2S_3: Structural, Optical, Electrical and Photoelectrochemical Properties. *Optik*, **126**, 5715-5717. https://doi.org/10.1016/j.ijleo.2015.09.083

[13] Li, R.J., Tang, L., Zhao, Q., Ly, T.H., Teng, K.S., Li, Y., Hu, Y., Shu, C. and Lau, S.P. (2019) Nano Express Open Access In_2S_3 Quantum Dots: Preparation, Properties and Optoelectronic Application. *Nanoscale Research Letters*, **14**, Article No. 161. https://doi.org/10.1186/s11671-019-2992-0

[14] Nehra, S.P., Chander, S., Sharma, A. and Dhaka, M.S. (2015) Effect of Thermal An-

nealing on Physical Properties of Vacuum Evaporated In_2S_3 Buffer Layer for Eco-Friendly Photovoltaic Applications. *Materials Science in Semiconductor Processing*, **40**, 26-34. https://doi.org/10.1016/j.mssp.2015.06.049

[15] Timoumi, A., Bouzouita, H. and Rezig, B. (2013) Characterisation and Wemple-Didomenico Model of Indium Sulphide Thin Layers for Photovoltaic Applications. *Australian Journal of Basic and Applied Sciences*, **7**, 448-456.

[16] Rasool, S., Reddy, G.P., Reddy, K.T.R., Tivanov, M. and Gremenok, V.F. (2017) Effect of Substrate Temperature on Structural and Optical Properties of In_2S_3 Thin Films Grown by Thermal Evaporation. *Materials Today*: *Proceedings*, **4**, 12491-12495. https://doi.org/10.1016/j.matpr.2017.10.049

[17] Assili, K., Selmi, W., Alouani, K. and Vilanova, X. (2019) Computational Study and Characteristics of In_2S_3 Thin Films: Effects of Substrate Nature and Deposition Temperature. *Semiconductor Science and Technology*, **34**, Article ID: 045006. https://doi.org/10.1088/1361-6641/ab0446

[18] John, T.T., Mathew, M., Kartha, C.S., Vijayakumar, K.P., Abe, T. and Kashiwaba, Y. (2005) $CuInS_2/In_2S_3$ Thin Film Solar Cell Using Spray Pyrolysis Technique Having 9.5% Efficiency. *Solar Energy Materials and Solar Cells*, **89**, 27-36. https://doi.org/10.1016/j.solmat.2004.12.005

[19] Asenjo, B., Chaparro, A.M., Gutiérrez, M.T., Herrero, J. and Maffiotte, C. (2005) Study of the Electrodeposition of In_2S_3 Thin Films. *Thin Solid Films*, **480**-**481**, 151-156. https://doi.org/10.1016/j.tsf.2004.11.023

[20] Timoumi, A., Bouzouita, H. and Rezig, B. (2011) Optical Constants of Na-In_2S_3 Thin Films Prepared by Vacuum Thermal Evaporation Technique. *Thin Solid Films*, **519**, 7615-7619. https://doi.org/10.1016/j.tsf.2011.01.410

[21] Bouguila, N., Timoumi, A. and Bouzouita, H. (2014) Vacuum Annealing Temperature on Spray In_2S_3 Layers. *The European Physical Journal Applied Physics*, **65**, Article No. 20304. https://doi.org/10.1051/epjap/2014130341

[22] Abdelkader, D., Khemiri, N. and Kanzari, M. (2013) The Effect of Annealing on the Physical Properties of Thermally Evaporated $CuIn_{2n+1}S_{3n+2}$ Thin Films (n=0, 1, 2 and 3). Effect of Annealing on the Structural and Optical Properties of In_2S_3 Films. *Materials Science in Semiconductor Processing*, **16**, 1997-2004. https://doi.org/10.1016/j.mssp.2013.07.029

[23] Bekheet, A.E. and El-Khawas, E.H. (2013) Effect of Annealing on the Structural and Optical Properties of In_2S_3 Films. *International Journal of Scientific & Engineering Research*, **4**, 1-7.

[24] Strohm, A., Eisenmann, L., Gebhardt, R.K., Harding, A., Schlotzer, T., Abou-Ras, D. and Schock, H.W. (2005) $ZnO/In_xS_y/Cu(In,Ga)Se_2$ Solar Cells Fabricated by Coherent Heterojunction Formation. *Thin Solid Films*, **480**-**481**, 162-167. https://doi.org/10.1016/j.tsf.2004.11.032

[25] Naghavi, N. Henriquez, R. Laptev, V. and Lincot, D. (2004) Growth Studies and Characterization of In_2S_3 Thin Films Deposited by Atomic Layer Deposition (ALD). *Applied Surface Science*, **222**, 65-73. https://doi.org/10.1016/j.apsusc.2003.08.011

[26] Gorai, S., Guha, P., Ganguli, D. and Chaudhuri, S. (2003) Chemical Synthesis of β-In_2S_3 Powder and Its Optical Characterization. *Materials Chemistry and Physics*, **82**, 974-979. https://doi.org/10.1016/j.matchemphys.2003.08.013

[27] Swanepoel, R. (1982) Determination of the Thickness and Optical Constants of Amorphous Silicon. *Journal of Physics E*: *Scientific Instruments*, **16**, 1214-1218. https://doi.org/10.1088/0022-3735/16/12/023

[28] Pankove, J.I. (1971) Optical Processes in Semiconductors. Prentice-Hall, Englewood

Cliffs, NJ, 18-23.

[29] Prabakar, K., Venkatachalam, S., Jeyachandran, Y.L., Narayandass, S.K. and Mangalaraj, D. (2004) Optical Constants of Vacuum Evaporated $Cd_{0.2}Zn_{0.8}Te$ Thin Films. *Solar Energy Materials and Solar Cells*, **81**, 1-12. https://doi.org/10.1016/j.solmat.2003.08.008

[30] Chopra, K.L. (1969) Thin Film Phenomena. McGraw-Hill, New York, 118-126.

[31] Samantha, B., Sharma, S.L. and Chaudhuri, A.K. (1994) Optical and Micro Structural Properties of $Cd_{0.2}Zn_{0.8}Te$ Thin Films. *Indian Journal of Pure & Applied Physics*, **32**, 62-67.

[32] Gupta, V. and Mansingh, A. (1996) Influence of Post Deposition Annealing on the Structural and Optical Properties of Sputtered Zinc Oxide Film. *Journal of Applied Physics*, **80**, 1063-1073. https://doi.org/10.1063/1.362842

[33] Vijayakumar, G.N.S., Rathnakumari, M. and Sureshkumar, P. (2011) Synthesis, Dielectric, AC Conductivity and Non-Linear Optical Studies of Electrospun Copper Oxide Nanofibers. *Archives of Applied Science Research*, **3**, 514-525.

[34] Tompkins, H.G. and McGahan, W.A. (1999) Spectroscopic Ellipsometry and Reflectometry. John Wiley & Sons Inc., New York, 12-18.

[35] Wemple, S.H. and DiDomenico, M. (1971) Behavior of the Electronic Dielectric Constant in Covalent and Ionic Materials. *Physical Review B*, **3**, 1338-1351. https://doi.org/10.1103/PhysRevB.3.1338

[36] Wemple, S.H. (1973) Refractive-Index Behavior of Amorphous Semiconductors and Glasses. *Physical Review B*, **7**, 3767-3777. https://doi.org/10.1103/PhysRevB.7.3767

[37] Li, M., Tu, X., Wang, Y., *et al.* (2018) Highly Enhanced Visible-Light-Driven Photoelectrochemical Performance of ZnO Modified In_2S_3 Nanosheet Arrays by Atomic Layer Deposition. *Nano-Micro Letters*, **10**, Article No. 45. https://doi.org/10.1007/s40820-018-0199-z

[38] Wang, L., Xia, L., Wu, Y. and Tian, Y. (2016) Zr-Doped β-In_2S_3 Ultrathin Nanoflakes as Photoanodes: Enhanced Visiblelight-Driven Photoelectrochemical Water Splitting. *ACS Sustainable Chemistry & Engineering*, **4**, 2606-2614. https://doi.org/10.1021/acssuschemeng.6b00090

[39] Liu, F., Jiang, Y., Yang, J., *et al.* (2016) MoS_2 Nanodots Decorated In_2S_3 Nanoplates: A Novel Heterojunction with Enhanced Photoelectrochemical Performance. *Chemical Communications*, **52**, 1867-1870. https://doi.org/10.1039/C5CC09601D

[40] Sankir, N.D., Aydin, E. and Sankir, M. (2014) Impedance Spectroscopy and Dielectric Properties of Silver Incorporated Indium Sulfide Thin Films. *International Journal of Electrochemical Science*, **9**, 3864-3875.

[41] Bouguila, N., Najeh, I., Ben Mansour, N., Bouzouita, H. and Alaya, S. (2015) AC Conductivity Properties of Annealed In_2S_3 Film Deposited by Spray Technique. *Journal of Materials Science: Materials in Electronics*, **26**, 6471-6477. https://doi.org/10.1007/s10854-015-3238-2

[42] Raj Mohamed, J., Sanjeeviraja, C. and Amalraj, L. (2016) Effect of Substrate Temperature on Nebulized Spray Pyrolysised In_2S_3 Thin Films. *Journal of Materials Science: Materials in Electronics*, **27**, 4437-4446. https://doi.org/10.1007/s10854-016-4315-x

[43] Mohameda, J.R. and Amalraj, L. (2016) Effect of Precursor Concentration on Physical Properties of Nebulized Spray Deposited In_2S_3 Thin Films. *Journal of Asian Ceramic Societies*, **4**, 357-366. https://doi.org/10.1016/j.jascer.2016.07.002